Flexible Printed Circuit Board as Novel Electrodes for Acoustofluidic Devices

Chao Sun, Roman Mikhaylov, Yongqing Fu, Fangda Wu, Hanlin Wang, Xichen Yuan, Zhihua Xie, Dongfang Liang, Zhenlin Wu, Xin Yang

Abstract*—Surface acoustic wave (SAW) based acoustofluidics shows broad applications in biomedicine and chemistry. Conventional manufacturing process for SAW devices uses photolithography and metal deposition, thus requires accessing cleanroom facilities. This study presents an efficient and versatile technique based on a flexible printed circuit board (FPCB) for developing SAW acoustofluidic devices. By mechanically clamping interdigital electrodes (IDEs) made on the FPCB onto a piezoelectric substrate, SAWs can be effectively generated with an additional matching network. The SAW amplitudes was measured by a laser vibrometer, which increases with the applied input voltage. The FPCB-SAW device has been applied to actuate 10-μm microspheres to form strong streaming vortices inside a droplet, and to drive a sessile droplet for transportation on the substrate surface. The use of the FPCB rather than a rigid PCB can help cut down on the overall footprint of the device and save space. The low requirement in assembling the FPCB-SAW device can facilitate versatile acoustofluidic applications by providing fast prototyping devices.

***Index Terms*— acoustofluidics, surface acoustic wave, flexible printed circuit board, interdigital electrode, droplet.**

I. INTRODUCTION

SURFACE acoustic wave (SAW) based acoustofluidics , as a continuous-flow, label-free and non-contact tool, has been widely applied in manipulating micro- and nano-particles [1, 2], circulating tumor cells [3], exosomes [4, 5], single cells [6] and human embryotic stem cells [7]. One of the most commonly used substrates for fabricating SAW device is lithium niobate (LiNbO₃) due to its large electro-mechanical coupling coefficient [8, 9]. SAW based devices are generally fabricated by patterning interdigitated transducers (IDTs) onto the LiNbO₃ substrate employing photolithography techniques involving the following steps done in cleanroom: mask manufacturing, spin-coating photoresist onto LiNbO₃, mask aligning for patterning with a UV light source, pattern development, metal layer deposition and lift-off process to form the IDT [10]. The IDT patterning requires a number of high-profile instrumentations such as mask aligner and sputter [11]. The patterned IDT is a permanent component, any modification to the IDT requires going through the entire manufacturing processes again.

Alternative techniques for making SAW devices were reported. Stacking aluminum foil strips onto the LiNbO₃ substrate using surface contact is demonstrated to produce low frequency acoustic Lamb waves [12]. Ref. [13] also reported a low-cost method to pour a low-melting point metal liquid into an IDT mold made by polydimethylsiloxane (PDMS) to form electrodes. A more accurate manufacturing technique was achieved by clamping a rigid printed circuit board (PCB) with a finger electrode pattern onto a LiNbO₃ substrate to make an acoustic tweezer with the ability to manipulate polystyrene microspheres and cancer cells [14]. PCBs show robustness to be used as electrodes for SAW devices, and its manufacture can be easily outsourced to process metal tracks using industrially mature technique. Apart from rigid PCBs, flexible PCBs (FPCBs), consisting of conductive circuit patterns coated on a thin insulating polymer film, are most important interconnection technologies in use for most advanced electronic products. Comparing with rigid PCBs, FPCBs have advantages such as dynamic flexing, less weight and better heat dissipation, which make them an ideal option for making SAW devices working on extreme temperatures and vibrations [15]. FPCBs can also increase the package density of the chip and create a more integrated design, with the potential of building three-dimensional and flexible transducer structures.

Previously, SAW devices manufactured on flexible ZnO/Al foil [16, 17] and BaTiO3/PVDF composite film [18] demonstrated great flexibility to generate both Lamb and

R.M., F.W., H.W., X.Y. are with the Department of Electrical and Electronic Engineering, School of Engineering, Cardiff University, UK CF24 3AA, (corresponding author Xin Yang, e-mail: yangx26@cf.ac.uk).

C.S., X.Y. are with School of Life Sciences, Northwestern Polytechnical University, 710072, P.R. China (e-mail: chaosun@nwpu.edu.cn, xichen.yuan@nwpu.edu.cn)

Y.F., is with the Faculty of Engineering and Environment, Northumbria University, Newcastle Upon Tyne, UK NE1 8ST (e-mail: richard.fu@northumbria.ac.uk)

Z.X., is with the Department of Civil Engineering, School of Engineering, Cardiff University, UK CF24 (e-mail: ZXie@cardiff.ac.uk)

D.L., is with the Department of Engineering, University of Cambridge, UK CB2 1PZ (e-mail: dl359@cam.ac.uk)

Z.W., is with the School of Optoelectronic Engineering and Instrumentation Science, Dalian University of Technology, 116023, P.R. China (e-mail: zhenlinwu@dlut.edu.cn)

Rayleigh waves. In this study, we demonstrated an acoustofluidic device made by using the FPCB. The novel device offered versatility, miniaturization and overcame the complex device structure and assembly requirement for the rigid PCB. The advantage of using the FPCB-SAW device also includes the evenness and effectiveness when the FPCB was in contact with the piezoelectric substrate during device assembly. Electrical properties of the FPCB-SAW device were systematically characterized, and the vibration patterns were quantified using a laser vibrometer. A parametric comparison was done with the rigid PCB performance, which resulted in a good agreement but the FPCB-SAW device saved on the overall footprint and required less assembling effort. The acoustofluidic performance of the FPCB-SAW device was verified by acoustic streaming and droplet transportation which underpin the FPCB-SAW device for wider applications.

II. METHODS AND MATERIALS

A. Device fabrication

The FPCB was fabricated (by circuitfly.com) using a standard PCB manufacturing process by patterning interdigital electrodes (IDEs) made of metal bilayers (Au/Ni, 30 nm/2 μm) onto a 70-μm thin polyester laminate (Fig. 1(a)). The IDEs on the FPCB consist of 40 pairs of 20-mm long finger electrodes. The designed finger width and spacing were both 50 μm, thus producing a SAW wavelength of 200 μm on LiNbO$_3$. A coaxial cable was soldered to the busbars of the IDEs. As schematically illustrated in Figs. 1(a) and 1(b), a 128° YX cut LiNbO$_3$ wafer (3-inch in diameter and 0.5 mm in thickness) was firstly placed onto a 2-mm thick aluminum sheet serving as a supporting board. Then the FPCB was mechanically pressed onto the LiNbO$_3$ wafer using an aluminum holder. At the IDT active area, a thin silicone pad was placed between the FPCB and the holder, to firmly press the finger electrodes to contact with the LiNbO$_3$ wafer. By fastening two side screws using a digital screwdriver, the force applied to the FPCB by the clamping unit of the aluminum holder and the silicone pad, namely the clamping force, could be adjusted to change the degree of proximity of the parts and the quality factor of the IDT. Fig. 1(b) shows the device configuration including the use of power meters for monitoring forward and reflected powers.

B. Device characterization

As shown in Fig. 1(b), an LC impedance matching network (shielded in the housing in Fig. 1(a)) was applied to match the impedance between the power amplifier and the FPCB-SAW device. The use of the matching network is essential for the device as it minimizes the reflection of the RF power [19] to allow the power amplifier work safely and improve the conversion of SAWs. A vector network analyzer (VNA, E5061B ENA, Keysight, USA) was used to measure the reflection coefficient S_{11} of the device with and without the matching network. The amplitude and phase of the S_{11} were measured. The Rayleigh mode frequency was identified as the frequency corresponding to the minimum S_{11} on the spectrum. The minimum S_{11} and the Rayleigh mode frequency in the

association of the clamping force applied on the FPCB was monitored by the VNA while the digital screwdriver (Adema, Taiwan) was fastening the screws. The torque reading from the screwdriver was used to calculate the clamping force [14]. The measurement was repeated three times for every clamping force. To minimize the signal reflection for enhancing the energy transmission and actuation effects, the screws were fastened at the position where the minimum S_{11} is reached, thus obtaining the minimum reflection. To demonstrate the repeatability and reproducibility of the FPCB-SAW device, the Rayleigh mode frequency and minimum S_{11} were measured by reassembling each FPCB-SAW device for 5 times. There were in a total of five FPCB-SAW devices developed to observe the device variation. The laser vibrometer (PSV-500-VH, Polytec, Germany) was used to characterize the surface vibration patterns and quantify the amplitude of the SAWs produced on the device. The maximum amplitudes of the surface vibration at various input powers with and without the matching network were characterized. Three measurements were acquired for each input power.

To quantify the influence of temperature and humidity on the Rayleigh mode frequency, the FPCB-SAW device was placed in a temperature-humidity chamber, in which the temperature and humidity can be set from 30 °C to 100 °C, and from 20 % to 90 %, respectively. The S_{11} spectra were recorded when varying the temperature at the fixed relative humidity (RH) of 50 %, and varying the humidity at room temperature.
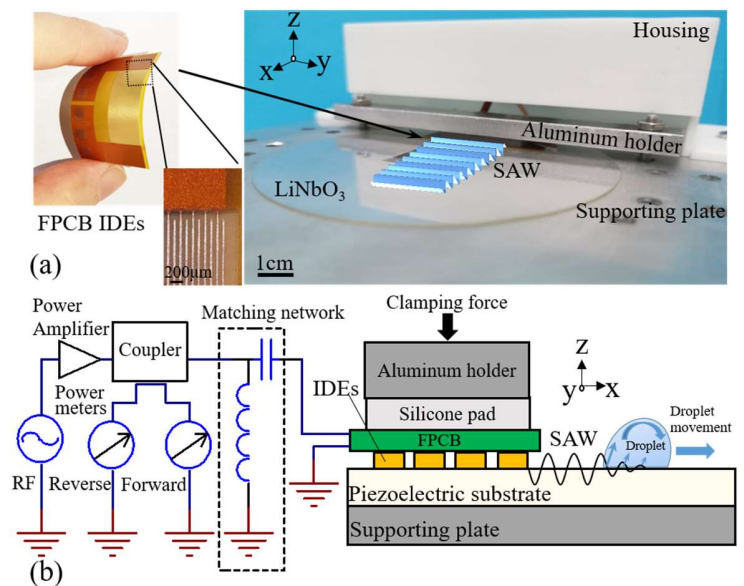

Fig. 1. (a) A photo of the FPCB IDEs and the FPCB-SAW device consisting of a FPCB stacked on a LiNbO$_3$ substrate. (b)The assembly diagram of the SAW generation on the FPCB- SAW device and its driving circuitry.

C. Acoustofluidics characterization

Before testing SAW interactions with droplets and polystyrene microspheres, a hydrophobic surface was created by coating a layer of CYTOP^{TM} (Asahi Glass Co. LTD, Japan) on the surface of the piezoelectric substrate. To demonstrate

streaming effect under different viscosities in the formation of micro-vortices, 10-μm polystyrene microspheres (Sigma-Aldrich, Germany) in two suspensions made of a mixture of glycerol and phosphate buffered saline (PBS) at the weight ratios of 3:7 and 9:1, respectively, were prepared. A droplet of the sample was placed on the hydrophobic area anterior to the finger electrode. For these tests, the input RF powers were set to 22 dBm and 25 dBm, respectively. To demonstrate pumping effect, a 1-μl sessile droplet of distilled water was placed on the SAW pathway and excited at a series of input powers. At each power, the droplet pumping experiment repeated three times and videos were recorded. The droplet transportation velocity was measured by using a video analysis tool (Tracker, OSP).

III. RESULTS AND DISCUSSION

As shown in Figs. 1(a-b), the jig of the FPCB-SAW device is much simpler comparing with that of the rigid PCB-SAW device [14]. The contact between the FPCB and the $LiNbO_3$ substrate is enabled by the aluminum holder and the silicone pad. The configuration is superior to the PCB-SAW device as it opens up a free space above the SAW region for accommodating other systems such as microfluidics while the previous rigid PCB-SAW device employed a sophisticated ring holder which fully occupied the device space. The aluminum holder is bolted by two M3 screws whose tightness directly controls the device frequency response. As a thin film material, the FPCB can be easily pressed by the silicone pad to compensate any roughness of the finger surface to enable better surface contact between the finger electrodes and the $LiNbO_3$ substrate. It did not require a well-tuned or evenly distributed pressure applied on the PCB for producing good electrical conductivity as the rigid PCB-SAW device. The FPCB can be flexibly bolted to any location on any piezoelectric substrates by the similar holder to generate customised SAW whose wavelength, propagation direction and amplitude are fully controllable. The FPCB-SAW device can be further miniaturised to offer a highly versatile and robust tool for wider acoustofluidic applications.

Fig. 2(a) shows the amplitude and phase of the reflection coefficient S_{11} of the FPCB-SAW device with and without using the matching network. The reflection coefficient S_{11} measures the power dissipation during the transmission over the total input source power [20] and a smaller value of S_{11} indicates more power coupled into the SAW device [21]. A minimum S_{11} is identified at 19.654 MHz when the matching network is used, which corresponds to the Rayleigh mode frequency determined by the wavelength of 200 μm and the speed of sound of $LiNbO_3$ of 3,990 $m·s^{-1}$. The matching network significantly reduces the minimum S_{11} from -7.29 dB to -47.12 dB and sets the phase close to zero leading to the device input impedance in a good match with the output impedance of the power amplifier (50 Ω). The slight working frequency shift with and without the matching network may be introduced by the additional inductance and capacitance from the LC network.
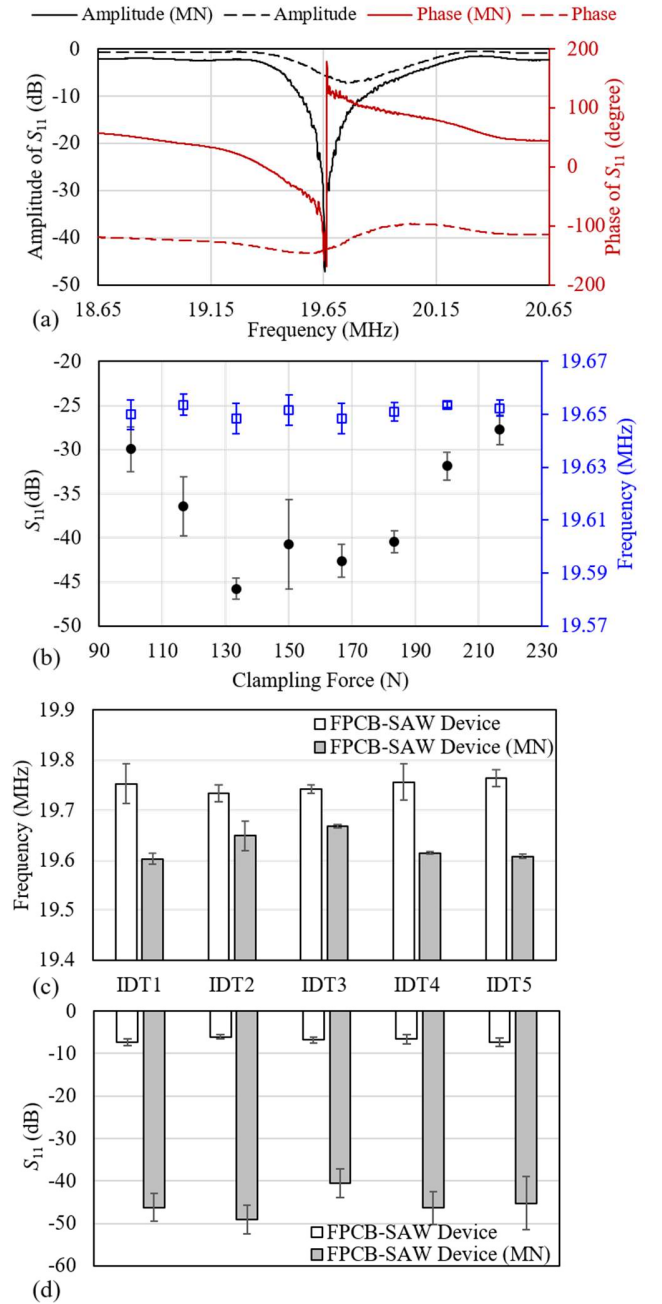

Fig. 2. Characterization of the FPCB-SAW device. (a) The amplitude and phase of the reflection coefficient S_{11} of the FPCB-SAW device with and without the matching network (MN). (b) The relationship between the S_{11} / the Rayleigh mode frequency and the clamping force. The reproducibility in (c) the Rayleigh mode frequency and (d) the minimum S_{11} of the reassembly of the FPCB-SAW device with and without the MN.

The data of minimum S_{11} and the Rayleigh mode frequency was recorded as a function of the clamping force between the FPCB and the $LiNbO_3$. As shown in Fig. 2(b), fastening the two M3 screws initially increases the clamping force and reduces the minimum value of S_{11} until the clamping force achieves around 133 N, where an optimal contact between the FPCB and the $LiNbO_3$ is reached. Further increasing the clamping force deteriorates the minimum S_{11} value due to the deformation of the FPCB at large forces. There exists an optimal clamping force to offer a minimum S_{11} for SAW

operation, which suggests monitoring S_{11} on the VNA to inform the completion of screw fastening. When the clamping force achieves 150 N, a bigger error bar is noted, this may be the result of that the S_{11} reading becomes very sensitive when the optimal state is achieved. Any small variation in the clamping force can lead to a large change in the S_{11}. Other potential factors such as the surface roughness / finishing of the substrate and finger electrodes could affect the relationship between the S_{11} and clamping force. These potential factors seem to be mitigated by the FPCB-SAW device owing to its unique structure and dynamic flexing, which is underpinned by that the minimum S_{11} of -47.12 dB is in a similar scale as that of a conventional SAW device made through photolithography. Fig. 2b also shows that increasing the clamping force does not notably vary the Rayleigh mode frequency.

The assembly repeatability with respect to the Rayleigh mode frequency and minimum S_{11} is shown in Figs. 2c and 2d. Each assembly was done at the optimal clamping force read by the S_{11}. Both variations in the Rayleigh mode frequency with and without the matching network are within 0.03 MHz, with the average frequencies of 19.63 MHz and 19.75 MHz, respectively. The variations in the minimum S_{11} value with and without the matching network are -6.79±1.06 dB and -45.49±6.20 dB, respectively, which indicates that the FPCB-SAW device has good reproducibility and small inter-device variability.

over a relative humidity range of 20-90 %. The inset is the Rayleigh frequency versus the relative humidity.

The influence of the temperature and the humidity on the Rayleigh mode frequency of the FPCB-SAW device are shown in Figs. 3a and 3b, respectively. The Rayleigh mode frequency in general decreases with the temperature rise, from 19.65 MHz to 19.57 MHz when the temperature ranged from 30 ℃ to 100 ℃. The varying humidity shows no obvious frequency shift over a RH range from 20 % to 90 % at room temperature. The characteristic response of the FPCB-SAW device to both temperature and humidity found similar to conventional SAW devices [22].

Fig. 4(a) shows the amplitudes and patterns of the surface vibration of the FPCB-SAW device working at an input voltage of 1.25 V on the Rayleigh mode. The sampling region is 788 μm×435 μm locating at ~5 mm anterior to the first finger electrode. The vibration amplitude and traveling pattern of the SAW is visualized on the surface of the LiNbO₃ where the acoustic amplitude is gradually diminished along the propagation from the right to left [23]. Fig. 4(b) shows the amplitudes of the surface vibration of the FPCB-SAW device at a series of input voltages with and without the use of the matching network. At 1.25 V, the vibration amplitude is 214.1 pm with the matching network, which is larger than the amplitude of 130.8 pm without the matching network. The improvement in the SAW amplitude when the matching network in place confirms the better reflection coefficient S_{11} is achieved as shown in Fig. 2(a).

(a)

(b)

Fig. 4. Surface vibration of the FPCB-SAW device. (a) The vibration pattern of the SAW traveling on the surface at the input voltage of 1.25 V. (b) The comparison of the maximum SAW amplitude of the FPCB-SAW device with and without the matching network at a series of the input signals.
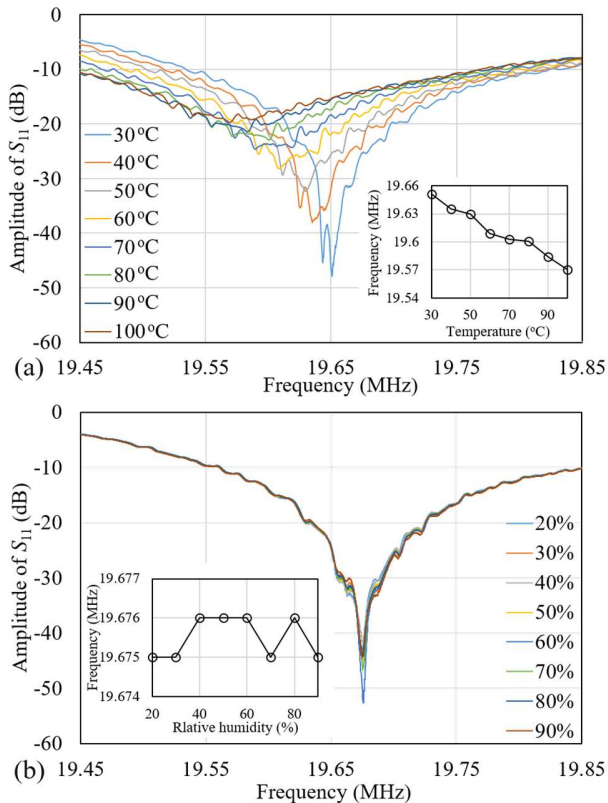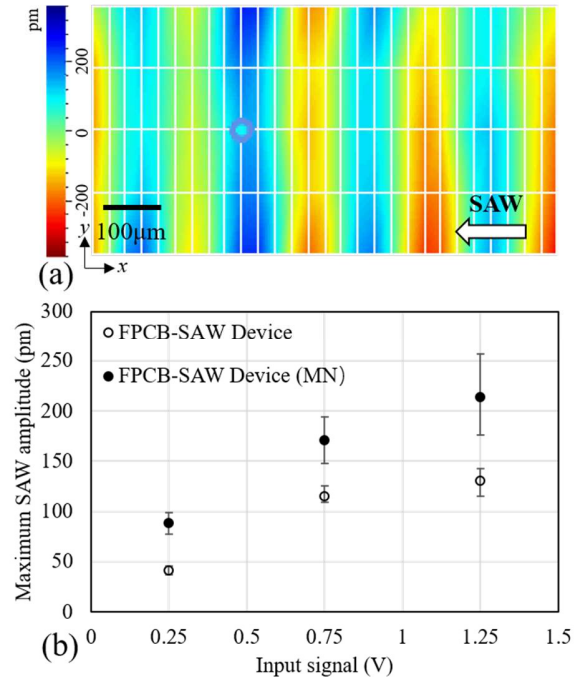

(a)

(b)

Fig. 3. Temperature and humidity tests of the FPCB-SAW device. (a) The amplitude of S_{11} changes with respect to the frequency over a temperature range of 30-100 ℃. The inset is the varying Rayleigh mode frequency versus the temperature. (b) The amplitude of S_{11} changes with respect to the frequency

Figs. 5(a) and 5(b) show the streaming patterns of 10-μm polystyrene microspheres within 12.5-μl droplets of high (glycerol/PBS = 3/7) and low viscosity (glycerol/PBS = 1/9) solutions, respectively, placed at a distance of 1 cm away from the first finger electrode of the FPCB-SAW device. Videos are

provided in Supplementary File. The produced vortex patterns of acoustic streaming are in good agreement with those created by using conventional SAW devices [24, 25]. Due to the differences in acoustic attenuation and Reynolds number of the medium, the viscosity of the liquid determines the micro-vortices to be either four-vortex or two-vortex [26]. In terms of input signals, the higher viscosity requires the higher input power of 25 dBm to effectively actuate the microspheres, comparing with 22 dBm for the low viscosity sample.
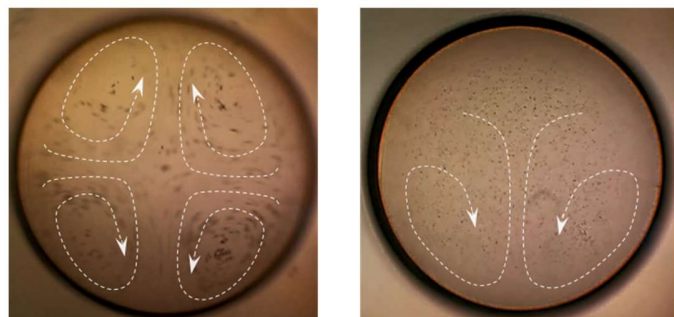
(a)　　　　　　　　　　　(b)

Fig. 5. Acoustic streaming produced by the FPCB-SAW device. (a) Four microsphere micro-vortices are produced within a droplet with low viscosity, the input power is 22 dBm. (b) Two microsphere micro-vortices are produced within a droplet with high viscosity, the input power is 25 dBm
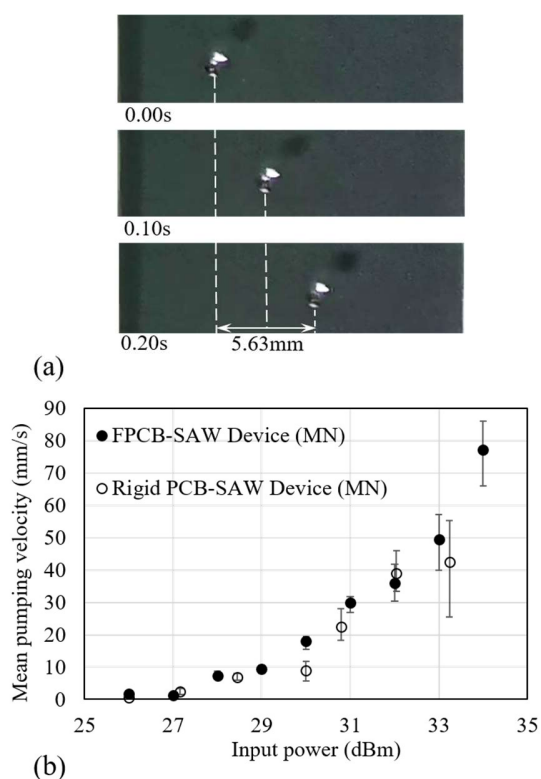

(a)

(b)

Fig. 6. Droplet transportation on the FPCB-SAW device. (a) Images of droplet transportation driven by the SAW at 31 dBm with the mean velocity of 29.79mm/s. (b) Comparison of the pumping velocity of a droplet between the FPCB-SAW device and the rigid PCB-SAW device at different input powers.

Droplet transportation developed from acoustic pumping and jetting typically represents SAW actuation on piezoelectric substrates [27, 28]. Fig. 6(a) shows examples of efficient transportation of a 1-μl droplet using the FPCB-SAW device. Using the input power of 31 dBm, the droplet transportation

velocity is 29.79 ± 2.60 mm·s^{-1}. Fig. 6(b) shows that the mean pumping velocity of the droplet in association with the input power. By applying the input power from 26 dBm to 34 dBm, the pumping velocity increases from 1.73 mm/s to 77.17 mm/s, which indicates the SAW amplitude is well controlled by the input power. The trend of the pumping velocity is compared with that of the previous rigid PCB-SAW device [14]. In general, the pumping velocity is slightly higher on the FPCB-SAW device, which could be the result of an optimal mechanical contact between the FPCB and the LiNbO$_3$. The simplified jig for assembling the FPCB-SAW device is able to perform droplet and particle manipulation comparable to the rigid PCB-SAW device and conventional SAW device made by photolithography.

IV. CONCLUSION

This paper reports a novel acoustofluidic device based on FPCB with much simpler device structure and assembling process. It inherits the advantages of our previous rigid PCB-SAW device including easy fabrication and low-skill entry. The FPCB-SAW device employs flexible finger electrodes to stack onto piezoelectric substrates. The power consumption of the FPCB-SAW device is similar to that of the rigid version, while the whole device involves only a few mechanical components off the shelf offering larger flexibility for integrating with microfluidics or other systems. In addition, the FPCB itself has merits in mechanical flexibility, reduction of weight and space, dynamic flexing and less assembly effort, which requests less resources in acoustofluidic microfabrication. The characterization and tests of the FPCB-SAW device using microparticles and droplet indicate its versatility and potential in prototyping acoustofluidic devices for wider applications.

REFERENCE

[1]   Z. Ma, D. J. Collins, J. Guo, and Y. Ai, "Mechanical properties based particle separation via traveling surface acoustic wave," *Analytical Chemistry,* vol. 88, no. 23, pp. 11844-11851 2016, DOI: 10.1021/acs.analchem.6b03580

[2]   Z. Mao, P. Li, M. Wu, H. Bachman, N. Mesyngier, X. Guo, S. Liu, F. Costanzo, and T. J. Huang, "Enriching Nanoparticles via Acoustofluidics," *ACS Nano,* vol. 11, no. 1, pp. 603-612 2017, DOI: 10.1021/acsnano.6b06784

[3]   M. Wu, P. H. Huang, R. Zhang, Z. Mao, C. Chen, G. Kemeny, P. Li, A. V. Lee, R. Gyanchandani, A. J. Armstrong, M. Dao, S. Suresh, and T. J. Huang, "Circulating Tumor Cell Phenotyping via High-Throughput Acoustic Separation," *Small,* vol. 14, no. 32, 2018, DOI: 10.1002/smll.201801131

[4]   M. Wu, Y. Ouyang, Z. Wang, R. Zhang, P. H. Huang, C. Chen, H. Li, P. Li, D. Quinn, M. Dao, S. Suresh, Y. Sadovsky, and T. J. Huang, "Isolation of exosomes from whole blood by integrating acoustics and microfluidics," *Proceedings of the National Academy of Sciences of the United States of America,* vol. 114, no. 40, pp. 10584-10589 2017, DOI: 10.1073/pnas.1709210114

[5]   Z. Wang, F. Li, J. Rufo, C. Chen, S. Yang, L. Li, J. Zhang, J. Cheng, Y. Kim, M. Wu, E. Abemayor, M. Tu, D. Chia, R. Spruce, N. Batis, H. Mehanna, D. T. W. Wong, and T. J. Huang, "Acoustofluidic Salivary Exosome Isolation: A Liquid Biopsy Compatible Approach for Human Papillomavirus–Associated Oropharyngeal Cancer Detection," *The Journal of Molecular Diagnostics,* vol. 22, no. 1, pp. 50-59 2020/01/01/. 2020, DOI: https://doi.org/10.1016/j.jmoldx.2019.08.004

[6]   D. J. Collins, B. Morahan, J. Garcia-Bustos, C. Doerig, M. Plebanski, and A. Neild, "Two-dimensional single-cell patterning

with one cell per well driven by surface acoustic waves," *Nature Communications,* vol. 6, p. 8686 2015, DOI: 10.1038/ncomms9686

[7] M. C. Zalis, J. F. Reyes, P. Augustsson, S. Holmqvist, L. Roybon, T. Laurell, and T. Deierborg, "Label-free concentration of viable neurons, hESCs and cancer cells by means of acoustophoresis," *Integrative Biology (United Kingdom),* vol. 8, no. 3, pp. 332-340 2016, DOI: 10.1039/c5ib00288e

[8] J. Shi, X. Mao, D. Ahmed, A. Colletti, and T. J. Huang, "Focusing microparticles in a microfluidic channel with standing surface acoustic waves (SSAW)," *Lab on a Chip,* vol. 8, no. 2, pp. 221-223 2008, DOI: 10.1039/b716321e

[9] Z. Tian, S. Yang, P.-H. Huang, Z. Wang, P. Zhang, Y. Gu, H. Bachman, C. Chen, M. Wu, Y. Xie, and T. J. Huang, "Wave number–spiral acoustic tweezers for dynamic and reconfigurable manipulation of particles and cells," *Science Advances,* vol. 5, no. 5, p. eaau6062 2019, DOI: 10.1126/sciadv.aau6062

[10] X. Ding, Z. Peng, S.-C. S. Lin, M. Geri, S. Li, P. Li, Y. Chen, M. Dao, S. Suresh, and T. J. Huang, "Cell separation using tilted-angle standing surface acoustic waves," *Proceedings of the National Academy of Sciences,* vol. 111, no. 36, pp. 12992-12997 2014, DOI: 10.1073/pnas.1413325111

[11] C. Sun, F. Wu, D. J. Wallis, M. H. Shen, F. Yuan, J. Yang, J. Wu, Z. Xie, D. Liang, H. Wang, R. Tickle, R. Mikhaylov, A. Clayton, Y. Zhou, Z. Wu, Y. Fu, W. Xun, and X. Yang, "Gallium Nitride: A Versatile Compound Semiconductor as Novel Piezoelectric Film for Acoustic Tweezer in Manipulation of Cancer Cells," *IEEE Transactions on Electron Devices,* vol. 67, no. 8, pp. 3355-3361 2020, DOI: 10.1109/TED.2020.3002498

[12] A. R. Rezk, J. R. Friend, and L. Y. Yeo, "Simple, low cost MHz-order acoustomicrofluidics using aluminium foil electrodes," *Lab on a Chip,* vol. 14, no. 11, pp. 1802-1805 2014, DOI: 10.1039/C4LC00182F

[13] Z. Ma, A. J. T. Teo, S. H. Tan, Y. Ai, and N. T. Nguyen, "Self-aligned interdigitated transducers for acoustofluidics," *Micromachines,* vol. 7, no. 12, 2016, DOI: 10.3390/mi7120216

[14] R. Mikhaylov, F. Wu, H. Wang, A. Clayton, C. Sun, Z. Xie, D. Liang, Y. Dong, F. Yuan, D. Moschou, Z. Wu, M. H. Shen, J. Yang, Y. Fu, Z. Yang, C. Burton, R. J. Errington, M. Wiltshire, and X. Yang, "Development and characterisation of acoustofluidic devices using detachable electrodes made from PCB," *Lab on a Chip,* vol. 20, no. 10, pp. 1807-1814 2020, DOI: 10.1039/C9LC01192G

[15] P. Macleod, *A Review of Flexible Circuit Technology and its Applications.* Loughborough, Leics: PRIME Faradya Partnership, 2002.

[16] Y. Liu, J. T. Luo, C. Zhao, J. Zhou, S. A. Hasan, Y. Li, M. Cooke, Q. Wu, W. P. Ng, J. F. Du, Q. Yu, Y. Liu, and Y. Q. Fu, "Annealing Effect on Structural, Functional, and Device Properties of Flexible ZnO Acoustic Wave Sensors Based on Commercially Available Al Foil," *IEEE Transactions on Electron Devices,* vol. 63, no. 11, pp. 4535-4541 2016, DOI: 10.1109/TED.2016.2610466

[17] Y. Liu, Y. Li, A. M. el-Hady, C. Zhao, J. F. Du, Y. Liu, and Y. Q. Fu, "Flexible and bendable acoustofluidics based on ZnO film coated aluminium foil," *Sensors and Actuators B: Chemical,* vol. 221, pp. 230-235 2015/12/31/. 2015, DOI: https://doi.org/10.1016/j.snb.2015.06.083

[18] Y. Yang, H. Pan, G. Xie, Y. Jiang, C. Chen, Y. Su, Y. Wang, and H. Tai, "Flexible piezoelectric pressure sensor based on polydopamine-modified BaTiO3/PVDF composite film for human motion monitoring," *Sensors and Actuators A: Physical,* vol. 301, p. 111789 2020/01/01/. 2020, DOI: https://doi.org/10.1016/j.sna.2019.111789

[19] R. D. O'Rorke, C. D. Wood, C. Wälti, S. D. Evans, A. G. Davies, and J. E. Cunningham, "Acousto-microfluidics: Transporting microbubble and microparticle arrays in acoustic traps using surface acoustic waves," *Journal of Applied Physics,* vol. 111, no. 9, p. 094911 2012, DOI: 10.1063/1.4711101

[20] K. Kurokawa, "Power Waves and the Scattering Matrix," *IEEE Transactions on Microwave Theory and Techniques,* vol. 13, no. 2, pp. 194-202 1965, DOI: 10.1109/TMTT.1965.1125964

[21] R. Weser, A. Winkler, M. Weihnacht, S. Menzel, and H. Schmidt, "The complexity of surface acoustic wave fields used for microfluidic applications," *Ultrasonics,* vol. 106, p. 106160 2020/08/01/. 2020, DOI: https://doi.org/10.1016/j.ultras.2020.106160

[22] Y. Zhang, Q. Tan, L. Zhang, W. Zhang, and J. Xiong, "A novel SAW temperature-humidity-pressure (THP) sensor based on LiNbO(3)for environment monitoring," *Journal of Physics D-Applied Physics,* vol. 53, no. 37, Sep 9. 2020, DOI: 10.1088/1361-6463/ab9138

[23] C. Fu, Y. Ke, A. Quan, C. Li, X. Fan, J. Ou, and J. Luo, "Investigation of Rayleigh wave and Love wave modes in 112‾0 ZnO film based multilayer structure," *Surface and Coatings Technology,* vol. 363, pp. 330-337 2019, DOI: 10.1016/j.surfcoat.2019.01.090

[24] R. J. Shilton, M. Travagliati, F. Beltram, and M. Cecchini, "Nanoliter-droplet acoustic streaming via ultra high frequency surface acoustic waves," *Advanced Materials,* vol. 26, no. 29, pp. 4941-4946 2014, DOI: 10.1002/adma.201400091

[25] J. Zhou, H. F. Pang, L. Garcia-Gancedo, E. Iborra, M. Clement, M. De Miguel-Ramos, H. Jin, J. K. Luo, S. Smith, S. R. Dong, D. M. Wang, and Y. Q. Fu, "Discrete microfluidics based on aluminum nitride surface acoustic wave devices," *Microfluidics and Nanofluidics,* vol. 18, no. 4, pp. 537-548 2015, DOI: 10.1007/s10404-014-1456-1

[26] A. Riaud, M. Baudoin, O. Bou Matar, J. L. Thomas, and P. Brunet, "On the influence of viscosity and caustics on acoustic streaming in sessile droplets: an experimental and a numerical study with a cost-effective method," *Journal of Fluid Mechanics,* vol. 821, pp. 384-420 2017, DOI: 10.1017/jfm.2017.178

[27] X. Y. Du, M. E. Swanwick, Y. Q. Fu, J. K. Luo, A. J. Flewitt, D. S. Lee, S. Maeng, and W. I. Milne, "Surface acoustic wave induced streaming and pumping in 128° Y-cut LiNbO3for microfluidic applications," *Journal of Micromechanics and Microengineering,* vol. 19, no. 3, p. 035016 2009/02/18. 2009, DOI: 10.1088/0960-1317/19/3/035016

[28] M. H. Biroun, M. T. Rahmati, M. Jangi, R. Tao, B. X. Chen, and Y. Q. Fu, "Computational and experimental analysis of droplet transportation/jetting behaviours driven by thin film surface acoustic waves," *Sensors and Actuators A: Physical,* vol. 299, p. 111624 2019/11/01/. 2019, DOI: https://doi.org/10.1016/j.sna.2019.111624